Rare Met. (2022) 41(2):639–649
https://doi.org/10.1007/s12598-021-01759-4

RARE METALS

ORIGINAL ARTICLE

Flower-like CuS/graphene oxide with photothermal and enhanced photocatalytic effect for rapid bacteria-killing using visible light

Rui Lv, Yan-Qin Liang, Zhao-Yang Li*, Sheng-Li Zhu, Zhen-Duo Cui, Shui-Lin Wu*

Received: 26 January 2021 / Revised: 24 February 2021 / Accepted: 6 March 2021 / Published online: 7 June 2021

Abstract Pathogenic bacteria have been threatening the daily life of human beings. More effective methods without causing drug-resistance of bacteria need to be developed to fight against these pathogens. Herein, flower-like CuS/-graphene oxide (GO) hybrids have been successfully synthesized via simple one-pot hydrothermal process. GO worked as an excellent electron acceptor to transport the photogenerated electrons from CuS, which can suppress the recombination of hole–electron pairs efficiently, thus enhancing the photocatalytic property. In addition, the morphology of CuS and GO with high specific surface area and the increased defect in GO also improved photocatalytic performance of the hybrid. Owing to the synergy of photothermal, enhanced photocatalytic effect and released Cu ions, CuS/GO exhibited outstanding antibacterial efficacy under visible light irradiation for 15 min. Additionally, the hybrid showed great biocompatibility to L929 cell. Hence, the synthesized CuS/GO would be a promising antibacterial material for daily life including rapid water disinfection and wounds sterilization.

Keywords Antibacterial; Photocatalytic; CuS; Graphene oxide; Photoresponsive

1 Introduction

In daily life, pathogenic bacteria with great adaptability and high reproductive rate remain one of the biggest health challenges as a result of polluting food and drinking water or infecting wounds and implant devices, which may even lead to death of human beings [1, 2]. Since the discovery of penicillin by Fleming [3], many kinds of antibiotics have been discovered and developed to fight against pathogens as effective antimicrobial drugs by inhibiting DNA, RNA, cell wall or protein synthesis [4]. However, the misuse and overuse of them have already led to the appearance of drug-resistant bacteria and even the occurrence superbugs due to mutated genes of chromosome and horizontal gene transfer [5, 6]. It has been speculated by World Health Organization (WHO) that ~ 10 million people will die every year from diseases caused by bacterial resistance by 2050 [7]. The ongoing spread of multi-resistant bacteria requires novel alternative strategies to treat drug-resistant infections. So up to now, many scientists apply themselves to look for effective methods to solve this problem [8].

To date, various strategies have been proposed against pathogenic bacteria as the substitute of antibiotics by light, microwave and magnetism [9, 10]. Many studies have proved that Cu nanoparticles have antimicrobial activity against different species of bacteria, which have similar antibacterial properties but are cheaper than other expensive noble metals, like silver [11–13]. However, Cu

Supplementary Information The online version contains supplementary material available at https://doi.org/10.1007/s12598-021-01759-4.

R. Lv, Y.-Q. Liang, Z.-Y. Li*, S.-L. Zhu, Z.-D. Cui, S.-L. Wu*
School of Materials Science & Engineering, the Key Laboratory of Advanced Ceramics and Machining Technology by the Ministry of Education of China, Tianjin University, Tianjin 300072, China
e-mail: zyli@tju.edu.cn

S.-L. Wu
e-mail: shuilinwu@tju.edu.cn

R. Lv, Y.-Q. Liang, Z.-Y. Li, S.-L. Zhu, Z.-D. Cui, S.-L. Wu
The Key Laboratory of Advanced Ceramics and Machining Technology by the Ministry of Education of China, Tianjin University, Tianjin 300072, China

nanoparticles still have some disadvantages, especially rapid oxidation on exposure to air, limiting their applications [11]. Among lots of Cu-based particles, copper sulfide (CuS) is one of the important semiconductor materials, with narrow optical band gap energy depending on crystalline phase. It has attracted the attention of researchers for their excellent optical and electronic properties.

Photothermal therapy (PTT), which can convert optical energy from light irradiation into thermal energy and treat infections by high heat focusing on the bacterial infected area, had attracted persistent attention from scientists, because light can be controlled to a certain area and penetrate tissues without damage to health [14]. CuS, working as a typical photothermal agent, has a broad absorption and several advantages such as low cost, easy preparation and good biocompatibility [15, 16]. Photocatalytic therapy (PCT) is also a promising method for bacteria-killing, which can generate elevated reactive oxygen species (ROS), such as singlet oxygen, superoxide radicals, hydrogen peroxide, as well as hydroxyl radicals. It works by oxidation and/or reduction reactions from most semiconductors including CuS, causing damage to pathogen's essential macromolecules such as DNA, RNA and proteins [17, 18]. It revealed that the synergistic action of both ROS and heat can kill bacteria more efficiently than single factor alone [19]. Besides, it has been reported that ROS yields can be enhanced by the heating effects and released Cu ions from CuS [20]. Nowadays, CuS has been widely recognized as having promising availability in the antibacterial field including Gram-negative and Gram-positive bacteria. However, the easy recombination of the photo-excited holes and electrons, along with aggregation of itself, restricts the photocatalytic antibacterial efficiency of CuS [21, 22]. On the other hand, compared with traditional CuS, flower-like CuS is more famous because of their high surface-to-volume ratios and large specific surface area that has been widely used in the degradation of dyes, showing improved photocatalytic properties [23, 24], but rarely used in the antimicrobial field.

In recent decades, graphene, a famous carbon material, has been widely used for its high specific surface area due to the carbon atoms monolayer structure, which has always been doped to modify existing properties or endow new properties on demand [25, 26]. A lot of studies focused on graphene oxide (GO), one of graphene-based materials, for its low-cost synthesis and similar high surface area, which contains abundant oxygen functional groups, such as epoxy group, hydroxyl group and carboxyl group, and also having high electron mobility [27]. In view of this, we proposed a hypothesis whether the photocatalytic performance of CuS can be significantly enhanced by introducing GO sheet, which can not only suppress the aggregation of CuS, but also improve the photoelectron transfer efficiency, contributing to PCT.

Herein, we reported a simple one-pot method to synthesize flower-like CuS anchored on GO sheets, as schematically illustrated in Scheme 1. To select the appropriate quantity of GO, CuS/GO10, CuS/GO40 and CuS/GO70 with varied GO contents were prepared, all of whose photothermal and photocatalytic property were measured under visible light (0.2 $W \cdot cm^{-2}$).

2 Experimental

2.1 Synthesis of flower-like CuS

0.5 g copper (II) nitrate hydrate and 0.3 g thiourea were dissolved in a mixture solution containing 10 ml ethylene glycol and 30 ml deionized water. Next, 0.3 g hexadecyl trimethyl ammonium bromide (CTAB) was dissolved in the above solution under magnetic stirring for 30 min. Then, the mixture was placed into a 60 ml Teflon-lined autoclave and heated at 100 °C for 18 h. After reaction, the products were washed by distilled water (three times) and ethanol (three times), and then the flower-like CuS spheres were collected after dried in vacuum at 60 °C for 12 h.

2.2 Synthesis of flower-like CuS/GO

Cu^{2+} and GO were combined by electrostatic adsorption interaction. Surfaces of GO sheets, with highly negative charge when dispersed in water, can easily adsorb Cu^{2+} [28]. 10, 40 and 70 mg GO were dispersed in 30 ml deionized water under ultrasound for 1 h, and then 0.5 g copper (II) nitrate hydrate was added, respectively, stirring magnetically for 1 h. 0.3 g thiourea, 10 ml ethylene glycol and 0.3 g CTAB were added into the above solutions with 30 min magnetic stirring. The mixed solutions were reacted in 60 ml autoclave for 18 h at 100 °C. The final products were obtained after washed and dried, and the corresponding samples were labeled as CuS/GO10, CuS/GO40 and CuS/GO70.

2.3 Characterization

Surface morphology of samples was characterized by scanning electron microscopy (SEM, Hitachi S-4800). Elemental compositions and distributions were performed on energy-dispersive X-ray spectrometry (EDS, Oxford X-max20). X-ray diffraction (XRD) patterns were recorded on a DX-2700BH X-ray diffractometer. Elemental analysis was measured by X-ray photoelectron spectroscopy (XPS, Axis Supra). Ultraviolet–visible (UV–Vis) spectra were acquired using a UV-2700 with $BaSO_4$ as a reference. The

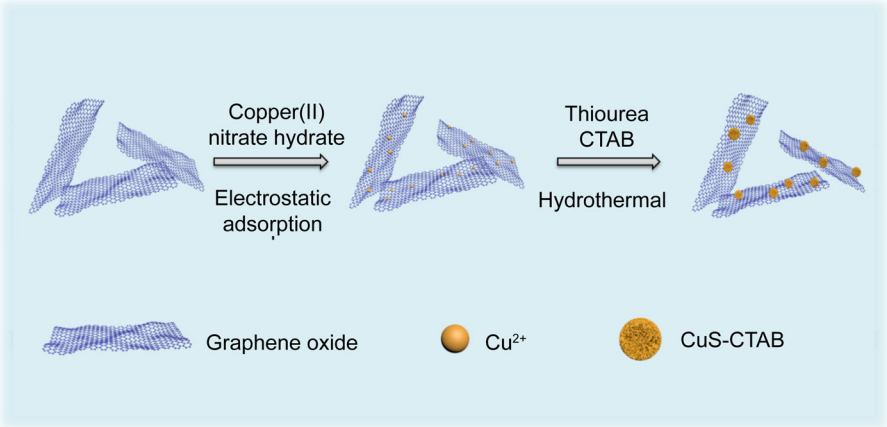

Scheme 1 Illustration of synthesis process of CuS/GO

functional groups were determined by a Fourier transform infrared spectrometer (FTIR, Nicolet iS10) and a Raman microscope (DXR2, Thermo Scientific). Simulated sunlight for anti-bacterial experiments was produced by a xenon lamp (PLS-SXE300).

2.4 Photothermal examination

CuS, CuS/GO10, CuS/GO40 and CuS/GO70 samples were put into a 96-well plate, and 160 μl PBS solution (pH 7.4) was added into the well. The xenon lamp (0.2 $W{\cdot}cm^{-2}$) was utilized to irradiate the samples, and the change of temperature was recorded every minute during 15 min according to a thermal camera (FLIR, E50).

To confirm the photothermal stability of CuS/GO70, the suspension was irradiated with light for 10 min and then without light to room temperature, which was repeated three times. The change of temperature was recorded every minute.

2.5 Electrochemical tests

Samples were used as the working electrode, while a Pt net worked as the counter electrode and Ag/AgCl worked as the reference electrode, reacting in the electrolyte of 0.1 $mol{\cdot}L^{-1}$ Na_2SO_4. The photocurrent measurements were performed with the visible light of 0.2 $W{\cdot}cm^{-2}$.

2.6 Antibacterial tests

Staphylococcus aureus (*S. aureus*) and *Escherichia coli* (*E. coli*) were used as experimental strains to reveal the antibacterial properties of samples. 160 μl 1×10^7 colony forming units (CFU)$\cdot ml^{-1}$ bacterial suspensions and 40 μl samples suspension (nutrient solution, CuS, CuS/GO10, CuS/GO40 and CuS/GO70) were added into a sterilized 96-well plate, respectively, while the final experimental concentration of the samples was 0.03%. After irradiated under light irradiation (0.2 $W{\cdot}cm^{-2}$) or in the dark for 15 min, the solutions were diluted 100 times and 20 μl of them were extracted and spread onto sterilized plates to cultivate at 37 °C for 24 h. The photographs of the plates were taken to calculate the antibacterial efficiency.

2.7 Effects of Cu^{2+}

160 μl bacterial suspensions were mixed, respectively, with 40 μl nutrient solution and CuS/GO70 were cultured in shaking table at 37 °C for 24 h, then diluted and spread onto sterilized plates at 37 °C for 24 h.

2.8 Morphological studies

To further observe the antibacterial ability of samples, the morphology of bacteria was examined by SEM. A sheet glass was placed into each 96-well plate before adding bacteria and samples suspensions with and without light irradiation. After 2 h at 4 °C for the mixture to sink, supernatant liquid was extracted out and the remaining bacteria on sheet glass were fixed with 2.5% glutaraldehyde solution for 40 min, followed by dehydrated with ethanol solutions (10%, 30%, 50%, 70%, 90% and 100%) for 15 min and then kept at 4 °C to dry for further observation by SEM.

2.9 Cytotoxicity evaluation

Using L929 fibroblasts as experimental cells, the cytotoxicity of samples was evaluated by cell counting kit-8 (CCK-8) at the same concentration of antibacterial tests. Firstly, samples were sterilized under the exposure to ultraviolet irradiation for 3 h and then added into the

culture medium for 1, 3 and 5 days, which would be used as new medium. In addition, cells were seeded in 96-well plates and cultured for 24 h. Different new mediums were added into the plates with cells for 1, 3 and 5 days, respectively. After that, medium was extracted and 10% CCK-8 solution was added to color the living cells, kept at 37 °C for 1 h. The optical density of living cells was obtained at 450 nm.

2.10 Statistic analysis

All of the experimental data were evaluated by means ± standard deviations at least three tests independently and performed by one-way analysis of variance. The p value < 0.05 was considered to be statistically significant.

3 Results and discussion

3.1 Characterization of flower-like CuS and CuS/GO

As shown in Fig. 1a, the as-synthesized CuS particles exhibited obvious flower-like sphere morphology with an average size of 1–3 μm, which were composed of nanoplates, and EDS results showed the signal of Cu and S with atomic ratio of about 1:1 (Fig. 1b). After hydrothermal reaction (Scheme 1), microspheres were in situ formed on the surface of GO nanosheets, and their numbers decreased as the initial content of GO increased (Fig. S1). High magnification image revealed that these microspheres were also composed of nanoplates with the same morphology and elemental ratio of Cu and S (Fig. 1c–e), indicating that the addition of GO did not change the morphology and composition of microspheres. TEM image showed that the in situ formed microspheres were closely contacted with GO nanosheets (Fig. 1f). HRTEM image (Fig. 1g) exhibited a lattice spacing of 0.27 nm, corresponding to the (006) plane of CuS [29]. SAED pattern further confirmed the formation of CuS on the surface of GO nanosheets (Fig. 1h). EDS mapping showed that Cu and S had almost the same distribution in the area of microsphere, while C and O showed uniform distribution, suggesting the existence of CuS microspheres on the surface of GO (Fig. S2). XRD was further utilized to analyze the phase composition of synthesized materials. As shown in Fig. 2a, the patterns of as-received GO showed a characteristic sharp diffraction (002) peak at $2\theta = 9.64°$ and a broad peak between 15° and

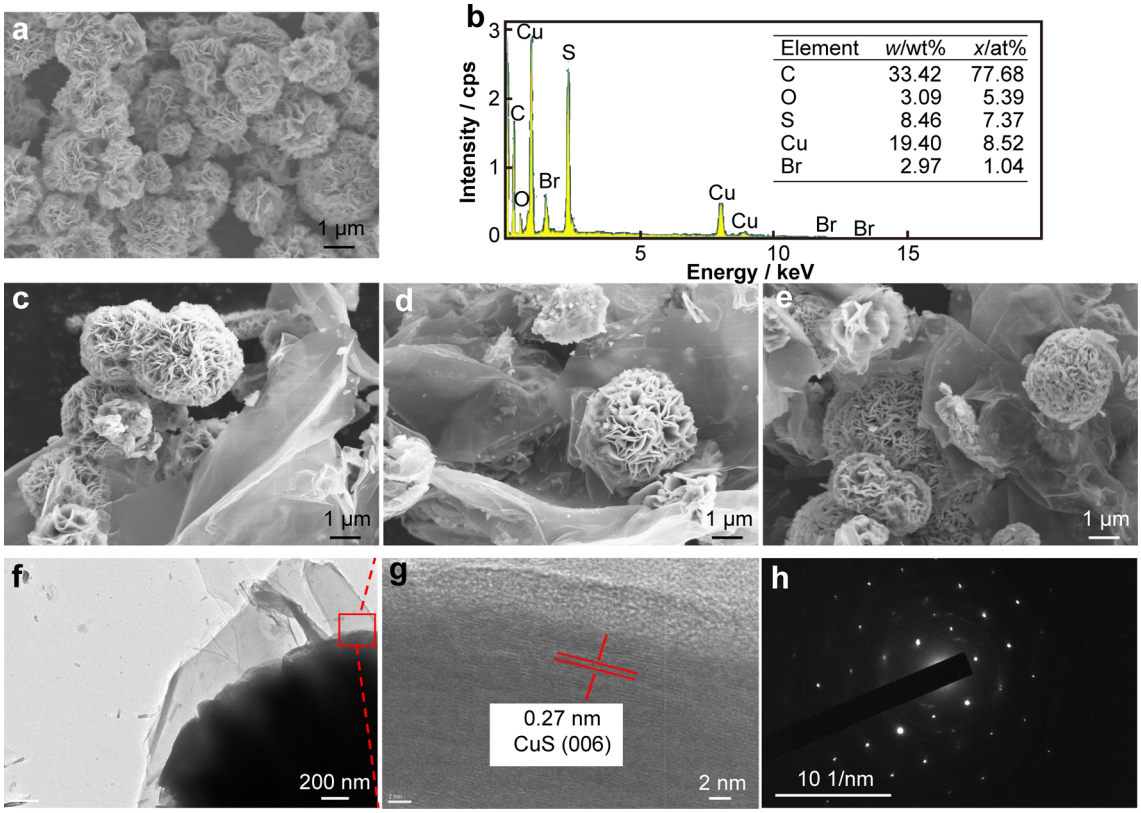

Fig. 1 Morphologies and compositions of synthesized samples: **a** SEM image of synthesized CuS; **b** EDS result of synthesized CuS; SEM image of synthesized **c** CuS/GO10, **d** CuS/GO40 and **e** CuS/GO70; **f** TEM image and **g** HRTEM image of synthesized CuS/GO70; **h** SAED pattern of **g**

25°, indicating the mixed phase of crystallized GO and some lower oxidation level of graphite [30, 31]. The diffraction peaks of as-prepared CuS were located at 27.08°, 29.18°, 31.90° and 47.58°, corresponding to the typical crystal faces of (101), (102), (105) and (107) of CuS [29], respectively. All hybrids of CuS/GO exhibited almost the same peaks as pristine CuS, indicating that the combination with GO did not change the phase structure.

The phase compositions of hybrids were further determined by FTIR and Raman spectrum. As shown in Fig. 2b, the FTIR spectrum obtained from the as-received GO showed characteristic vibration bands for the presence of O–H (3431 cm^{-1}), C=O (1732 cm^{-1}), C=C (1621 cm^{-1}), C–O–C (1382 cm^{-1}), confirming the GO phase with COOH and C–O–C and C–OH [32, 33]. Apart from these, the appearance of peak at 618 cm^{-1} related to Cu–S revealed the successful synthesis of CuS with GO [34]. The Raman spectrum of GO displayed particular D and G band peaks at 1349 and 1598 cm^{-1}, respectively (Fig. 2c). The former was evolved from the structural imperfections created by the sp^3C atom, while the latter could be attributed to the phonon vibrations from sp^2C atom [35]. Similarly, three kinds of CuS/GO hybrids also exhibited both D (1354 cm^{-1}) and G (1590 cm^{-1}) bands in corresponding Raman spectrum. The peak at 479 cm^{-1} also confirmed the existence of CuS [36]. The shift of D and G peaks possibly originated from the strong interaction between CuS and GO. Moreover, the D/G intensity ratio visibly increased, meaning the existence of more defects, which was beneficial for electronic transmission [37].

As shown in Fig. S3, distinctive XPS peaks of C 1s, O 1s, Cu 2p and S 2p could be found on CuS/GO powder. As

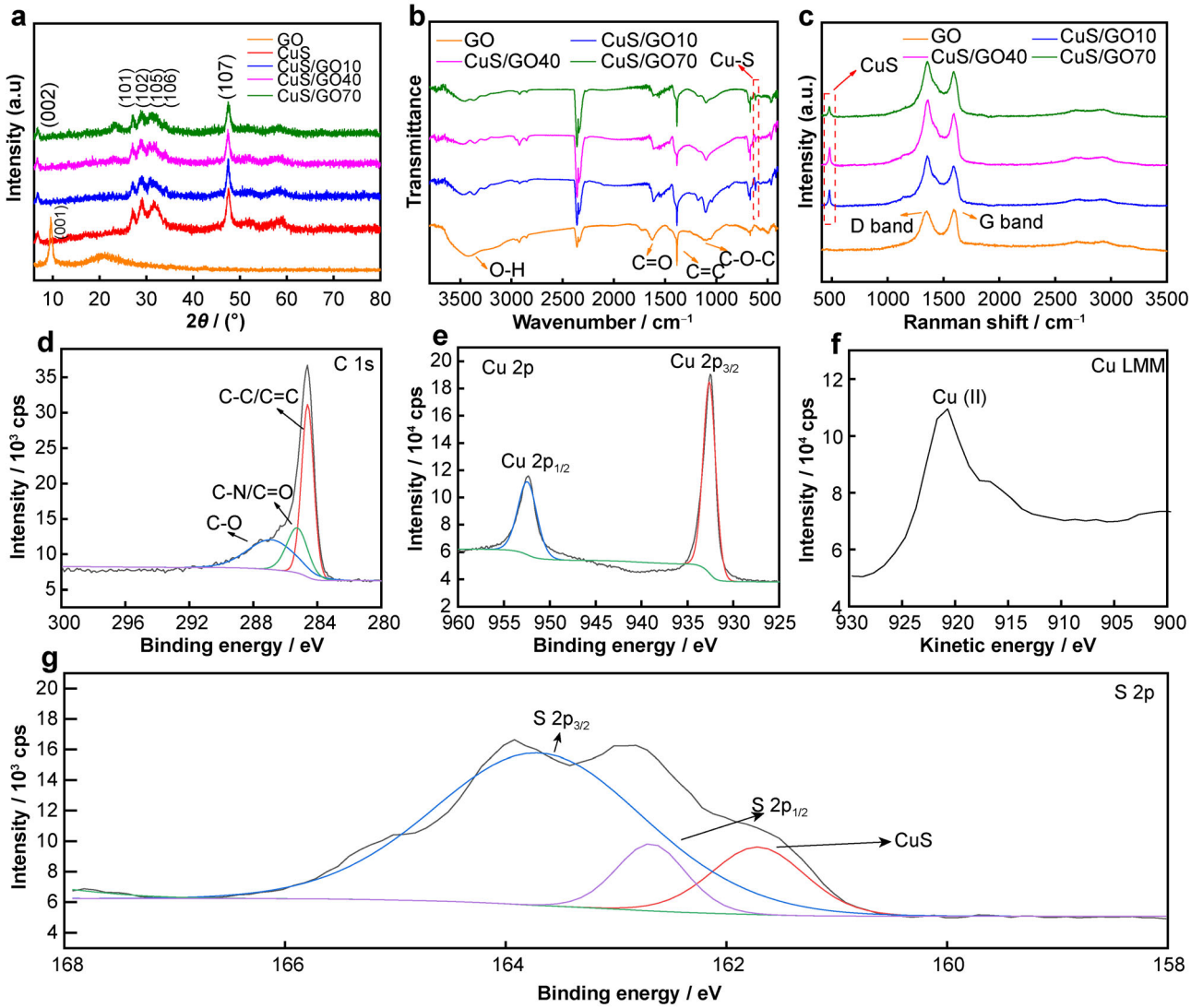

Fig. 2 Characterization of synthesized materials: **a** XRD patterns, **b** FTIR spectra, and **c** Raman spectra; XPS narrow scan of **d** C 1s, **e** Cu 2p, **f** Cu LMM and **g** S 2p obtained from CuS/GO powder

for the C 1s spectra of pure CuS, peaks at around 284.6, 286.1 and 288.5 eV could be assigned to C–C/C=C, C–O and C–N, respectively; while C–N was originated from CTAB (Fig. S4). For CuS/GO, peaks at around 284.6, 285.2 and 286.8 eV could be found, attributed to C–C/C=C, C–N/C=O and C–O bonding, respectively (Fig. 2d) [38–40]. As shown in Fig. 2e–f, two obvious peaks could be found in the spectra of Cu 2p at 932.6 and 952.5 eV, assigned to Cu $2p_{3/2}$ and Cu $2p_{1/2}$, respectively, while the corresponding kinetic energy of Cu LMM showed a maximum of the peak at 920.7 eV, belonging to the characteristic of Cu (II) of CuS [41]. S 2p spectra presented two strong peaks at 162.6 and 163.7 eV, assigned to S $2p_{3/2}$ and S $2p_{1/2}$ of S^{2-}, respectively. Besides, the side peak at 161.7 eV of CuS had been reported in previous studies [42]. XPS spectra showed that CuS/GO was successfully formed.

3.2 Photothermal performance

UV–Vis spectrum (Fig. 3a) could reflect the optical properties of samples in detail. Pure CuS showed excellent absorption capability from 200 to 800 nm. The wide absorption suggested the potential application of CuS for antibacterial use with full solar light. However, when cooperated with GO, CuS showed decreasing absorption, which became lower and lower with more and more GO added. The energy gap values of CuS, CuS/GO10, CuS/GO40 and CuS/GO70 were 1.12, 1.03, 0.98 and 0.90 eV, respectively (Fig. S5). Meanwhile, as shown in Fig. 3b, CuS could reach about 62 °C after 10-min light irradiation and kept for 5 min, while these composite samples exhibited rapidly rise to 52–54 °C, which were lower than pure CuS but could already have a certain destructive effect on bacteria. And the changes and differences could be observed from representative real-time thermal images (Fig. S6). Thus, CuS played the most important role in converting light into heat. Furthermore, to verify the photothermal stability of the composite, the laser on–off curve of CuS/GO70 was detected for three circles (Fig. 3c). When CuS/GO70 was exposed to light, its temperature rose up gradually and then cooled down to room temperature with light off. Figure 3c shows great photothermal stability of CuS/GO70 with basically consistent changes of temperature.

3.3 Photocatalytic performance

The photoelectron chemical experiment was carried out to determine the photocatalytic property of the samples. As the photocurrent curves shown in Fig. 4a, pure CuS showed minimal current, as a result of fast recombination of electron and hole, while all CuS/GO compositions exhibited significant increasing photocurrent density. Furthermore, the current of CuS was higher with more GO content added. Fig. S7 shows photoluminescence (PL) spectrum of the samples at room temperature, excited by wavelength of 350 nm. The PL spectrum of original CuS had emission at about 410 nm. The observed emissions intensity of compositions was changed as a result of subjoined GO. CuS/GO40 and CuS/GO70 with low PL intensity signified the low recombination rate of photo-induced charge carriers and hence higher photocatalytic property. Actually, GO was considered as an excellent electron acceptor and CuS can act as an electron donor, thus the composite effect between CuS and GO could efficiently suppress the recombination of hole–electron pairs in comparison with original CuS.

To acknowledge the existence of $\cdot O_2^-$ and ·OH, DMPO was used as spin trap detected by electron spin resonance spectrometers (ESR). ESR spectra (Fig. 4b) of CuS/GO70 were obtained with light irradiation and in dark. Six major characteristic peaks were attributed to the DMPO-$\cdot O_2^-$ adduct, while there was no existence of characteristic signal of DMPO-·OH adduct [43], indicating that superoxide radical played a major role during the photocatalytic process.

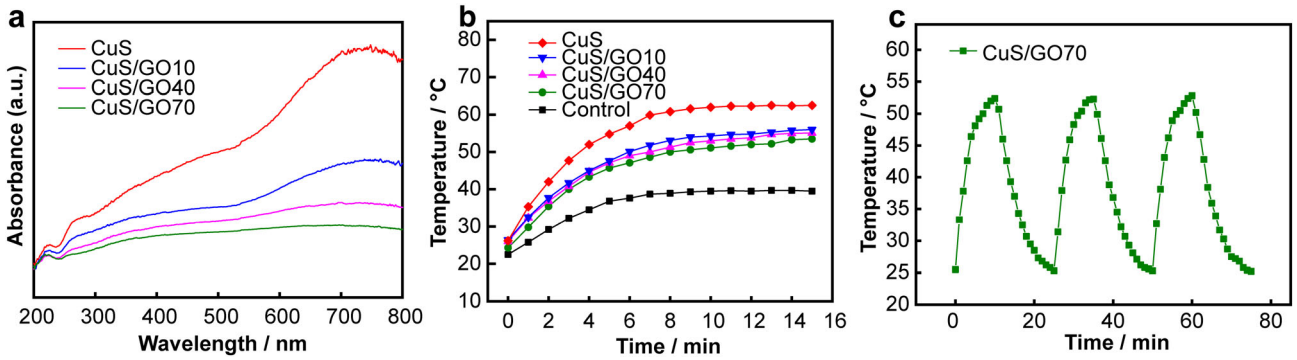

Fig. 3 Light absorption and photothermal properties of synthesized samples: **a** UV−Vis spectrum, **b** photothermal curves, and **c** photothermal stability curves of CuS/GO70

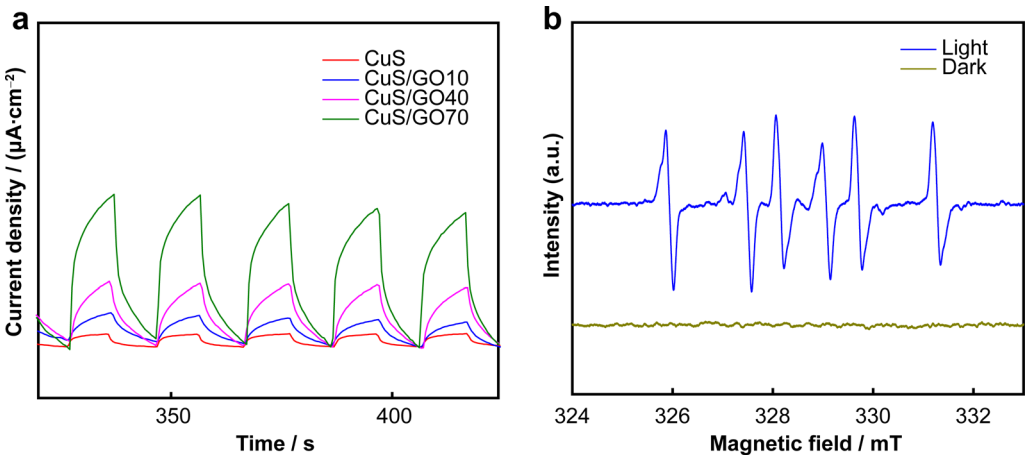

Fig. 4 Photoelectrochemical performance of samples: **a** photocurrent responses and **b** ESR spectra of CuS/GO70 with and without light irradiation

The valence band (VB) and conduction band (CB) potentials (E_{VB} and E_{CB}, respectively) of CuS can be approximately calculated based on the following equations, where E_C is the energy of free electrons on the hydrogen scale (about 4.5 eV), X means the electronegativity of the semiconductor, and E_g is the band gap of the semiconductor:

$$E_{CB} = X - E_C - E_g/2 \quad (1)$$

$$E_{VB} = E_{CB} + E_g \quad (2)$$

X (CuS) is about 5.29 eV and E_g of CuS is 1.12 eV obtained above, so the CB and VB potential of CuS are − 0.33 and 0.79 eV, respectively, the CB potential of CuS is equal to $E(O_2/\cdot O_2^-)$ (− 0.33 eV (vs. NHE)). However, its VB potential is more negative than $E(\cdot OH/H_2O)$ (2.4 eV (vs. NHE)), leading to holes unable to react with H_2O to produce ·OH [44].

Results above represented that the photocatalytic property of the CuS/GO composite was much better than that of CuS. The existence of GO prevented the recombination of the photogenerated electron and holes of CuS, thus enhancing photocatalytic property, consequently reducing more O_2 to $\cdot O_2^-$. At the same time, the morphology of CuS and GO with high specific surface area and the increased defect in GO were also conducive to photocatalytic effect. Except photocatalytic effect, the d-d transitions of Cu^{2+} in CuS can generate photothermal performance, along with the damage to bacteria of Cu^{2+} self [45, 46]. In conclusion, CuS/GO shows a great potential as a photothermal and photocatalytic agent for antibacterial applications, as illustrated in Fig. 5.

3.4 In vitro antibacterial property

In view of the compositions of CuS and GO exhibiting favorable property of photothermal and photocatalysis, they represented a huge potential for antibacterial activity against *S. aureus* and *E. coli*, which could be evaluated by spread plate method. As shown in Fig. 6a–d, the control group of PBS did not display any antibacterial effects regardless of irradiated by light or not. When in dark, samples did not show obvious antibacterial ability to *S. aureus*, while the antibacterial efficiency for *E. coli* was higher, which might be due to the different structures of them because the cell wall of *E. coli* is much thinner than that of *S. aureus* [2]. And these antibacterial results might be attributed to the released Cu ions when in dark, whose effect was further evaluated after culturing bacteria with CuS/GO70 for 24 h without light, and the results of bacterial counts reached 31.15% and 67.57% for *S. aureus* and *E. coli*, respectively (Fig. S8). When exposed to light, samples began to show great antibacterial effect. Photothermal effect of CuS could kill about 46.22% and 56.43% *S. aureus* and *E. coli*, respectively, and CuS/GO10, CuS/GO40 and CuS/GO70 acted better because of the improved photocatalytic property, although their reached temperature is lower than that of CuS after light irradition.

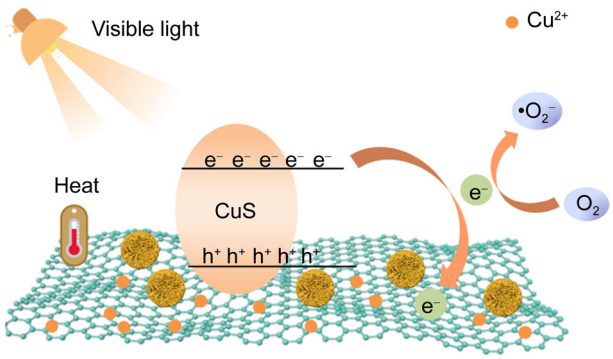

Fig. 5 Illustration of antibacerial mechanism of CuS/GO under visible light

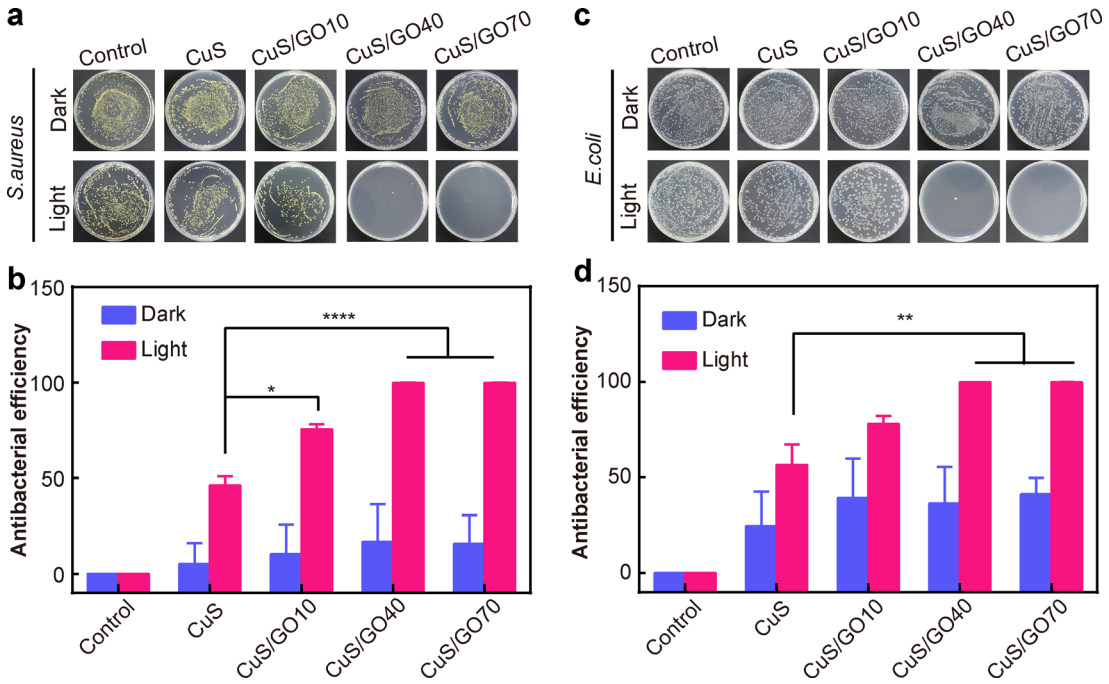

Fig. 6 Antibacterial activity of CuS, CuS/GO10, CuS/GO40 and CuS/GO70: spread plate of **a** *S. aureus* and **b** corresponding antibacterial efficiency; spread plate of **c** *E. coli* and **d** corresponding antibacterial efficiency (*$P < 0.05$, **$P < 0.01$, and ***$P < 0.001$)

Additionally, antibacterial efficiency of CuS/GO40 and CuS/GO70 could be measured to be 99.93% and 99.98% against *S. aureus* and 99.95% and 99.98% against *E. coli*, respectively. Therefore, the composite of CuS and GO improved the antibacterial property of pure CuS. And CuS/GO70 showed more excellent antibacterial activity than CuS/GO40.

SEM images of bacteria treated by GO, CuS and CuS/GO70 with and without light irradiation can be seen in Fig. 7a, b, consistent with the results of the spread plate. We found that *S. aureus* and *E. coli* incubated with PBS and GO remained smooth shape, demonstrating that the light treatment and GO alone had no damage to bacteria. However, when incubated with CuS, the morphology of both bacteria could be observed with slight deformation exposed to light, while those treated by CuS/GO70 were significantly disrupted and their contents released out. In comparison, when in dark, bacteria kept typical smooth shape with samples. Results above all proved the outstanding antibacterial property of CuS/GO70.

3.5 Cytotoxicity evaluation

In order to investigate the toxicity of samples, L929 was evaluated as a model through the CCK-8 assay for 1, 3 and 5 days. As shown in Fig. 8, pure CuS had already showed much damage to cell after co-cultivated for 1 day, because of excess release of Cu^{2+}. Meanwhile, CuS/GO composites displayed less damage to live cells due to the less released Cu^{2+} and their cell viability was 55.82%, 75.97% and 75.45%, respectively. Compared with that of pure CuS, cell viability of CuS/GO40 and CuS/GO70 was improved and showed great biocompatibility of 82.60% and 92.37% after 5 days, respectively. With long-term culture, both of them presented acceptable effect to cell and improved biocompatibility.

4 Conclusion

In this work, flower-like CuS/GO composites had been successfully synthesized via simple one-pot hydrothermal process with efficient antibacterial property and feasible toxicity. CuS had definitely PTT and PCT effect, but limited by the aggregation and easily recombined holes and electrons. To solve these problems, GO was added as electron transporter and a surface to suppress the aggregation of CuS, successfully enhancing the photocatalytic property. In addition, both the morphology of CuS and GO with high specific surface area and the increased defect in GO could improve the photocatalytic effect. CuS/GO70 exhibited outstanding antibacterial results under visible

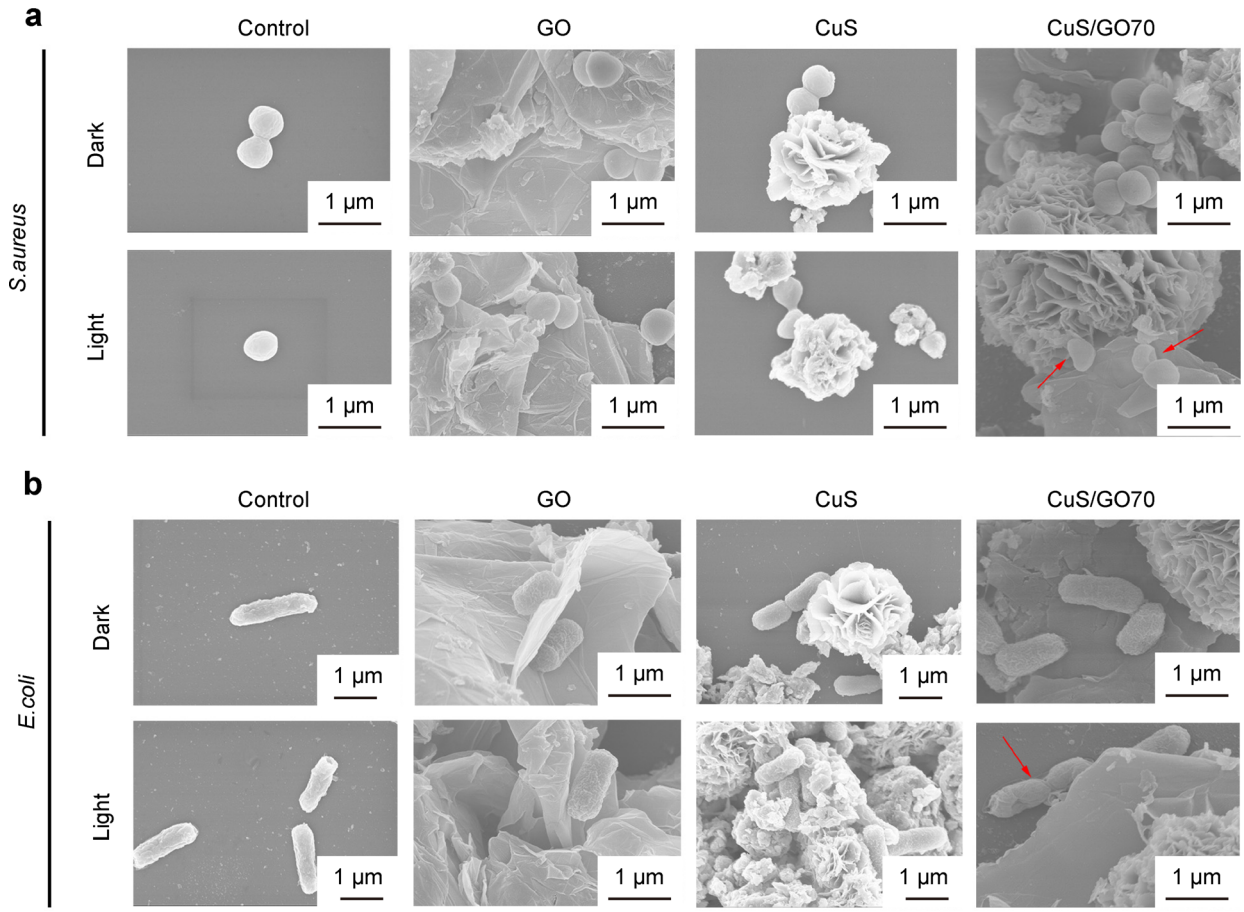

Fig. 7 SEM images of bacteria with GO, CuS and CuS/GO70: **a** *S. aureus* and **b** *E. coli*

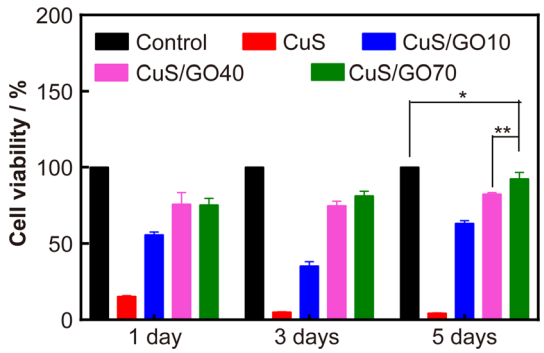

Fig. 8 CCK-8 assay of cell viabilities with different samples after co-cultured for 1, 3 and 5 days

light irradiation for 15 min and also showed great biocompatibility to L929 cell, thanks to synergy among PTT, enhanced PCT and released Cu ions, which can work effectively against bacteria from environment for both short and long antibacterial activity.

Acknowledgements This work was financially supported by the National Science Fund for Distinguished Young Scholars (No. 51925104) and the National Natural Science Foundation of China (Nos. 51871162 and 51671081)

References

[1] Xu JW, Yao K, Xu ZK. Nanomaterials with a photothermal effect for antibacterial activities: an overview. Nanoscale. 2019; 11(18):8680.
[2] Han D, Ma M, Han Y, Cui Z, Liang YQ, Liu XM, Li ZY, Zhu SL, Wu SL. Eco-friendly hybrids of carbon quantum dots modified MoS_2 for rapid microbial inactivation by strengthened photocatalysis. ACS Sustain Chem Eng. 2019;8(1):534.
[3] Ren Y, Han Y, Li Z, Liu X, Zhu S, Liang Y, Yeung KWK, Wu SL. Ce and Er co-doped TiO_2 for rapid bacteria-killing using visible light. Bioact Mater. 2020;5(2):201.
[4] Kohanski MA, Dwyer DJ, Collins JJ. How antibiotics kill bacteria: from targets to networks. Nat Rev Microbiol. 2010;8(6): 423.
[5] Yu P, Han YJ, Han DL, Liu XM, Liang YQ, Li ZY, Zhu SL, Wu SL. In-situ sulfuration of Cu-based metal-organic framework for rapid near-infrared light sterilization. J Hazard Mater. 2020;390: 122126.
[6] Blair JM, Webber MA, Baylay AJ, Ogbolu DO, Piddock LJ. Molecular mechanisms of antibiotic resistance. Nat Rev Microbiol. 2015;13(1):42.

[7] Ren Y, Liu HP, Liu X, Zheng YM, Li ZY, Li CY, Yeung KWK, Zhu SL, Liang YQ, Cui ZD, Wu SL. Photoresponsive materials for antibacterial applications. Cell Rep Phys Sci. 2020;1(11):100245.
[8] Laxminarayan R, Duse A, Wattal C, Zaidi AKM, Wertheim HFL, Sumpradit N. Antibiotic resistance—the need for global solutions. Lancet Infect Dis. 2013;13(12):1057.
[9] Cheeseman S, Christofferson AJ, Kariuki R, Cozzolino D, Daeneke T, Crawford RJ. Antimicrobial metal nanomaterials: from passive to stimuli-activated applications. Adv Sci (Weinh). 2020;7(10):1902913.
[10] Qiao YQ, Liu XM, Li B, Han Y, Zheng YF, Yeung KWK, Li CY, Cui ZD, Liang YQ, Li ZY, Zhu SL, Wang XB, Wu SL. Treatment of MRSA-infected osteomyelitis using bacterial capturing, magnetically targeted composites with microwave-assisted bacterial killing. Nat Commun. 2020;11(1):1.
[11] Usman MS, El Zowalaty ME, Shameli K, Zainuddin N, Salama M, Ibrahim NA. Synthesis, characterization, and antimicrobial properties of copper nanoparticles. Int J Nanomed. 2013;8:4467.
[12] Zhang EL, Fu S, Wang RX, Li HX, Liu Y, Ma ZQ, Liu GK, Zhu CS, Qin GW, Chen DF. Role of Cu element in biomedical metal alloy design. Rare Met. 2019;38(6):476.
[13] Rai M, Yadav A, Gade A. Silver nanoparticles as a new generation of antimicrobials. Biotechnol Adv. 2009;27(1):76.
[14] Jaque D, Martinez Maestro L, del Rosal B, Haro-Gonzalez P, Benayas A, Plaza JL, Rodriguez EM, Sole JG. Nanoparticles for photothermal therapies. Nanoscale. 2014;6(16):9494.
[15] Li M, Liu X, Tan L, Cui Z, Yang X, Li Z. Noninvasive rapid bacteria-killing and acceleration of wound healing through photothermal/photodynamic/copper ion synergistic action of a hybrid hydrogel. Biomater Sci. 2018;6(8):2110.
[16] Zhang X, Zhang G, Zhang H, Liu X, Shi J, Shi H. A bifunctional hydrogel incorporated with CuS@MoS_2 microspheres for disinfection and improved wound healing. Chem Eng J. 2020;382:122849.
[17] Tan L, Li J, Liu X, Cui Z, Yang X, Yeung KWK. In situ disinfection through photoinspired radical oxygen species storage and thermal-triggered release from black phosphorous with strengthened chemical stability. Small. 2018;14(9):1703197.
[18] Huang B, Tan L, Liu X, Li J, Wu S. A facile fabrication of novel stuff with antibacterial property and osteogenic promotion utilizing red phosphorus and near-infrared light. Bioact Mater. 2019;4(1):17.
[19] Xiong K, Li J, Tan L, Cui ZD, Li ZY, Wu SL, Liang YQ, Zhu SL, Liu XM. Ag_2S decorated nanocubes with enhanced near-infrared photothermal and photodynamic properties for rapid sterilization. Colloid Interface Sci Commun. 2019;33:100201.
[20] Li L, Rashidi LH, Yao M, Ma L, Chen L, Zhang J. CuS nanoagents for photodynamic and photothermal therapies: phenomena and possible mechanisms. Photodiagnosis Photodyn Ther. 2017;19:5.
[21] Wang Y, Jiang F, Chen J, Sun X, Xian T, Yang H. In situ construction of CNT/CuS hybrids and their application in photodegradation for removing organic dyes. Nanomaterials (Basel). 2020;10(1):178.
[22] Lucky SS, Soo KC, Zhang Y. Nanoparticles in photodynamic therapy. Chem Rev. 2015;115(4):1990.
[23] WangX HY, Hu Y, Jin G, Jiang B, Huang Y. Photothermal-conversion-enhanced photocatalytic activity of flower-like CuS superparticles under solar light irradiation. Sol Energy. 2018;170:586.
[24] Zhao L, Zhou L, Sun C, Gu Y, Wen W, Fang X. Rose-like CuS microflowers and their enhanced visible-light photocatalytic performance. CrystEngComm. 2018;20(41):6529.
[25] Mahmud RA, Shafawi AN, Ahmed Ali K, Putri LK, Md Rosli NI, Mohamed AR. Graphene nanoplatelets with low defect density as a synergetic adsorbent and electron sink for ZnO in the photocatalytic degradation of Methylene Blue under UV–Vis irradiation. Mater Res Bull. 2020;128:110876.
[26] Putri LK, Ng BJ, Ong WJ, Lee HW, Chang WS, Chai SP. Engineering nanoscale p–n junction via the synergetic dual-doping of p-type boron-doped graphene hybridized with n-type oxygen-doped carbon nitride for enhanced photocatalytic hydrogen evolution. J Mater Chem A. 2018;6(7):3181.
[27] Jo WK, Selvam NCS. Enhanced visible light-driven photocatalytic performance of ZnO-g-C_3N_4 coupled with graphene oxide as a novel ternary. J Hazard Mater. 2015;299:462.
[28] Yang X, Tu Y, Li L, Shang S, Tao XM. Well-dispersed chitosan/graphene oxide nanocomposites. ACS Appl Mater Interfaces. 2010;2(6):1707.
[29] Xiao Y, Su D, Wang X, Wu S, Zhou L, Shi Y. CuS microspheres with tunable interlayer space and micropore as a high-rate and long-life anode for sodium-ion batteries. Adv Energy Mater. 2018;8(22):1800930.
[30] Jeong HK, Lee YP, Lahaye RJWE, Park MH, An KH, Kim IJ, Yang CW, Park CY, Ruoff RS, Lee YH. Evidence of graphitic AB stacking order of graphite oxides. J Am Chem Soc. 2008;130(4):1362.
[31] Hanifah MFR, Jaafar J, Othman MHD, Ismail AF, Rahman MA, Yusof N. Facile synthesis of highly favorable graphene oxide: effect of oxidation degree on the structural, morphological, thermal and electrochemical properties. Materialia. 2019;6:100344.
[32] Yuxi X, Hua B, Gewu L, Chun L, Gaoquan S. Flexible graphene films via the filtration of water-soluble noncovalent functionalized graphene sheets. J Am Chem Soc. 2008;130(18):5856.
[33] Palanisamy S, Velmurugan S, Yang TCK. One-pot sonochemical synthesis of CuS nanoplates decorated partially reduced graphene oxide for biosensing of dopamine neurotransmitter. Ultrason Sonochem. 2020;64:105043.
[34] Baláž M, Dutková E, Bujňáková Z, Tóthová E, Kostova NG, Karakirova Y. Mechanochemistry of copper sulfides: characterization, surface oxidation and photocatalytic activity. J Alloys Compd. 2018;746:576.
[35] Zhu B, Lin B, Zhou Y, Sun P, Yao Q, Chen Y. Enhanced photocatalytic H_2 evolution on ZnS loaded with graphene and MoS_2 nanosheets as cocatalysts. J Mater Chem A. 2014;2(11):3819.
[36] Liu P, Huang Y, Yan J, Yang Y, Zhao Y. Construction of CuS nanoflakes vertically aligned on magnetically decorated graphene and their enhanced microwave absorption properties. ACS Appl Mater Interfaces. 2016;8(8):5536.
[37] Kuang Y, Shang J, Zhu T. Photoactivated graphene oxide to enhance photocatalytic reduction of CO_2. ACS Appl Mater Interfaces. 2020;12(3):3580.
[38] Chen C, Xu G, Wei X, Yang L. A macroscopic three-dimensional tetrapod-separated graphene-like oxygenated N-doped carbon nanosheet architecture for use in supercapacitors. J Mater Chem A. 2016;4(25):9900.
[39] Sitko R, Turek E, Zawisza B, Malicka E, Talik E, Heimann J. Adsorption of divalent metal ions from aqueous solutions using graphene oxide. Dalton Trans. 2013;42(16):5682.
[40] Liu J, Lin Z, Liu T, Yin Z, Zhou X, Chen S. Multilayer stacked low-temperature-reduced graphene oxide films: preparation, characterization, and application in polymer memory devices. Small. 2010;6(14):1536.
[41] Zuo ZJ, Li J, Han PD, Huang W. XPS and DFT studies on the autoxidation process of Cu sheet at room temperature. J Phys Chem C. 2014;118(35):20332.
[42] Fu W, Han W, Zha H, Mei J, Li Y, Zhang Z. Nanostructured CuS networks composed of interconnected nanoparticles for

asymmetric supercapacitors. Phys Chem Chem Phys. 2016; 18(35):24471.
[43] Ding H, Han D, Han Y, Liang Y, Liu X, Li Z. Visible light responsive CuS/ protonated g-C_3N_4 heterostructure for rapid sterilization. J Hazard Mater. 2020;393:122423.
[44] Lai C, Zhang M, Li B, Huang D, Zeng G, Qin L. Fabrication of CuS/$BiVO_4$ (040) binary heterojunction photocatalysts with enhanced photocatalytic activity for Ciprofloxacin degradation and mechanism insight. Chem Eng J. 2019;358:891.
[45] Chen J, Ning C, Zhou Z, Yu P, Zhu Y, Tan G. Nanomaterials as photothermal therapeutic agents. Prog Mater Sci. 2019;99:1.
[46] Zhang JM, Sun YH, Zhao Y, Liu YL, Yao XH, Tang B. Antibacterial ability and cytocompatibility of Cu-incorporated Ni–Ti–O nanopores on NiTi alloy. Rare Met. 2019;38(6):552.